HHS Public Access

Author manuscript

Cancer Lett. Author manuscript; available in PMC 2022 May 28.

Published in final edited form as:

Cancer Lett. 2021 May 28; 506: 107–119. doi:10.1016/j.canlet.2021.01.004.

Activating Sphingosine-1-phospahte signaling in endothelial cells increases myosin light chain phosphorylation to decrease endothelial permeability thereby inhibiting cancer metastasis

Yu-Chi Chen[1], **Saketh S. Dinavahi**[1], **Qilong Feng**[2], **Raghavendra Gowda**[1], **Srinivasa Ramisetti**[1], **Xinghai Xia**[2], **Kyle B LaPenna**[2], **Venkat R. Chirasani**[1], **Sung Hyun Cho**[12], **Susan L. Hafenstein**[8,13], **Madhu Babu Battu**[14], **Arthur Berg**[6], **Arun K. Sharma**[1], **Tom Kirchhausen**[15], **Nikolay V. Dokholyan**[1,7], **Shantu Amin**[1,*], **Pingnian He**[2,*], **Gavin P. Robertson**[1,3,4,5,7,9,10,11,*]

[1]Department of Pharmacology, The Pennsylvania State University College of Medicine, Hershey, PA 17033

[2]Department of Cellular and Molecular Physiology, The Pennsylvania State University College of Medicine, Hershey, PA 17033

[3]Department of Pathology, The Pennsylvania State University College of Medicine, Hershey, PA 17033

[4]Department of Dermatology, The Pennsylvania State University College of Medicine, Hershey, PA 17033

[5]Department of Surgery, The Pennsylvania State University College of Medicine, Hershey, PA 17033

[6]Department of Public Health Sciences, The Pennsylvania State University College of Medicine, Hershey, PA 17033

[7]Department of Biochemistry and Molecular Biology, The Pennsylvania State University College of Medicine, Hershey, PA 17033

[8]Department of Medicine, The Pennsylvania State University College of Medicine, Hershey, PA 17033

[9]Department of The Foreman Foundation for Melanoma Research, The Pennsylvania State University College of Medicine, Hershey, PA 17033

[10]Department of The Melanoma and Skin Cancer Center, The Pennsylvania State University College of Medicine, Hershey, PA 17033

Request for reprints: Gavin P. Robertson, Ph. D., Department of Pharmacology, The Pennsylvania State University College of Medicine, 500 University Drive, Hershey, PA 17033. Phone: (717) 531-8098; Fax: (717) 531-0480, gpr11@psu.edu, Pingnian He, Ph. D., Department of Cellular and Molecular Physiology, The Pennsylvania State University, College of Medicine, 500 University Drive, Hershey, PA 17033. Phone: (717)531-3596; Fax: (717)531-7667, pinghe@pennstatehealth.psu.edu, Shantu Amin, Ph. D., Department of Pharmacology, The Pennsylvania State University, College of Medicine, 500 University Drive, Hershey, PA 17033. Phone: (717) 531-1450; Fax: (717) 531 0244, sga3@psu.edu.

*Drs. Amin, He and Robertson share equal corresponding authorship.

Conflicts of interest: The authors declare no potential conflicts of interest.

[11]Department of The Melanoma Therapeutics Program, The Pennsylvania State University College of Medicine, Hershey, PA 17033

[12]The Huck Institutes of the Life Sciences, Pennsylvania State University, University Park, PA 16802

[13]Department of Biochemistry and Molecular Biology, Pennsylvania State University, University Park, PA 16802

[14]Department of Operon Diagnostics, Kompally, Hyderabad, India 500010

[15]Departments of Cell Biology, Harvard Medical School and Program in Cellular and Molecular Medicine at Boston Children's Hospital, MA, 02115

Abstract

Targeting the metastatic process to prevent disease dissemination in cancer remains challenging. One step in the metastatic cascade involves cancer cells transiting through the vascular endothelium after inflammation has increased the permeability of this cellular layer. Reducing inflammation-mediated gaps in the vascular endothelium could potentially be used to retard metastasis. This study describes the development of a novel ASR396-containing nanoparticle designed to activate the Sphingosine-1-Phosphate Receptor 1 (S1PR1) in order to tighten the junctions between the endothelial cell lining the vascular endothelium thereby inhibiting metastasis. ASR396 was derived from the S1PR1 agonist SEW2871 through chemical modification enabling the new compound to be loaded into a nanoliposome. ASR396 retained S1PR1 binding activity and the nanoliposomal formulation (nanoASR396) made it systemically bioavailable upon intravenous injection. Studies conducted in microvessels demonstrated that nanoASR396 significantly attenuated inflammatory mediator-induced permeability increase through the S1PR1 activation. Similarly, nanoASR396 inhibited gap formation mediated by inflammatory agents on an endothelial cell monolayer by decreasing levels of phosphorylated myosin light chain protein thereby inhibiting cellular contractility. In animal models, nanoASR396 inhibited lung metastasis by up to 80%, indicating its potential for retarding the melanoma metastasis. Thus, a novel bioavailable nanoparticle-based S1PR1 agonist has been developed to negate the effects of inflammatory mediators on the vascular endothelium in order to reduce the metastatic dissemination of cancer cells.

Keywords

Melanoma metastasis; inflammation; S1PR1; drug development; nanoliposomes

1. Introduction

Metastasis is the leading cause of cancer morbidity as well as mortality and is responsible for approximately 90% of cancer death (1–3). Metastasis is a general term to describe cancer cells traveling from primary sites to neighboring tissue or distant sites, which involves multiple steps including local invasion, intravasation, survival in circulation, extravasation, and proliferation in distant tissues (4). Each step can be rate-limiting since disruption of any of the multiple processes can retard metastasis (5).

The endothelial cell (EC) lining of vessels plays important roles during intravasation and extravasation in the metastatic cascade (6). While quiescent, non-activated ECs can reduce tumor cell transmigration and metastasis, inflammation increases gaps to facilitate these processes to promote cancer cell metastasis (7–9). The literature shows that melanomas and circulating tumor cells secrete multiple factors, such as thrombin, VEGF and monocyte chemoattractant protein 1 (MCP1/CCL2), which can disrupt endothelial layer integrity by triggering actin remodeling, cellular contractility and tight junctional disassembly (10–14).

Increases in vascular permeability mediated by inflammatory mediators can cause changes in EC junctions through modifications in adherens and tight junctions (15). Vascular endothelial (VE) cadherin at the edges of ECs plays a major role intracellularly linking actin filaments in the cytoskeleton (16). Inflammatory factors can cause internalization of VE-cadherin, whose absence then disrupts the cellular interactions leading to EC gap formation. In addition, contractile forces mediated by actin and myosin further promotes EC gap formation (17). The actin-myosin action depends on the phosphorylation status of myosin light chain (MLC) (18). Increased phosphorylated-MLC (pMLC) levels triggered by inflammatory mediators causes changes in the actin stress fibers leading to the formation of gaps in the EC layer (19).

Sphingosine-1-phosphate (S1P) is a natural lipid, and its levels in the plasma can be used as a biomarker for vascular barrier integrity (20). Cell culture studies showed that S1P enriched VE-cadherin and β-catenin at EC junctions; and enhanced adherens and tight junctional assembly (21). Studies in intact microvessels revealed that the effect of S1P on maintaining microvessel permeability occurred through the activation of EC S1PR1, and the blockage of S1PR1 abolished the inhibitory effect of S1P on inflammatory mediator-induced increases in microvessel permeability (22). Our study translates these observations to cancer treatment by developing a bioavailable S1PR1 agonist to enhance the endothelium barrier integrity and reverse the effects of inflammatory mediators, thereby inhibiting the transit of metastatic cells across vascular walls.

Several S1P receptor agonists have been developed for treating inflammatory diseases but none are useful for clinical cancer therapy (23). The most well-known S1P analog, FTY720 (fingolimod) is FDA-approved for treating multiple sclerosis but is not useful in cancer because it acts as a broad spectrum S1PR1/3/4/5 agonist (24). This leads to S1PR1 degradation and lymphopenia making it unsuitable to strengthen the endothelial barrier and reduce metastasis (25). SEW2871, a S1PR1-selective agonist, has been shown to fully replicate the action of S1P on endothelium integrity in intact microvessels, and potently inhibited the inflammatory mediator-induced increases in vascular permeability (22). Unfortunately, SEW2871 is not bioavailable requiring solubilization in a DMSO containing solution, which limits its clinical utility. The chemical structure of SEW2871 also prevents it from being incorporated into a bioavailable nanoliposomal formulation.

This report details the development of a bioavailable derivative of SEW2871 that acts as an agonist to S1PR1 to inhibit melanoma metastasis in preclinical models. The chemical structure of SEW2871 was modified to that of ASR396 so that it could be loaded into a nanoliposome but retained its ability to bind with and activate S1PR1. The nanoparticle

encapsulated ~70% of ASR396, had an average size of 69 nm, released 70% of ASR396 within 48 hours and was stable when refrigerated for 6 weeks. NanoASR396 was intravenously administered, making it instantly bioavailable in the blood circulation to inhibit EC gap formation mediated by inflammatory mediators. Mechanistically, it acted by reversing the levels of phosphorylated myosin light chain to reduce EC contractility. In animal models of metastasis, nanoASR396 inhibited lung metastasis by up to 80%, suggesting its potential for retarding the metastatic spread of melanoma.

2. Materials and Methods

2.1 Source, synthesis and characterization of compounds.

4-Phenyl-5-trifluoromethylthiophene-2-carboxylic acid (Fig. 1B, **compound 1**) and *N*-hydroxy-3-methoxy-benzamidine (Fig. 1B, **compound 2**) were purchased from Millipore Sigma. The purity of ASR396 (≥99%) was verified by analytical high-performance liquid chromatography (HPLC) analysis by comparing the peak areas of the product relative to any impurities. Specific synthesis and chemical characterization of ASR396 is described in the supplementary material and methods.

2.2 *In silico* binding assessment of ASR396 to ensure retention of interaction with S1PR1.

Crystal structure of S1PR1 receptor (PDB ID: 3V2W) was prepared and the active site pocket assigned as described previously (26). The crystal ligand in the active site pocket was examined with the various designed S1PR1 agonists and the docking interaction scores were calculated using the Glide module of the Schrodinger software.

2.3 Assessing ASR396 off-target binding.

The substructure-matching algorithm Erebus (erebus.doklab.org) was used to identify proteins featuring a similar or identical binding site to S1PR1. Erebus is a substructure-matching platform that is based on a select query of interatomic distances, which define a structural motif on a bait protein, performs a search of the entire RCSB protein database for all proteins featuring a similar or identical scaffold (27). Using Erebus, off-target proteins from the RCSB database were identified by matching substructures with the same amino acids and atoms separated by the same distances (within a given tolerance) as the atoms of the query structure. The accuracy of a match was measured by the root-mean-square deviation (RMSD) or by the normal weight with a given variance.

2.4 Development of a nanoliposome containing ASR396; nanoASR396.

A 80:20 mol % L-α-phosphatidylcholine (ePC) and 1,2-dipalmitoyl-sn-glycero-3-phosphoethanolamine-N-[methoxy(polyethylene glycol)-2000] ammonium salt (DPPE-PEG-2000) at a final concentration 25 mg/mL along with ASR396 (in methanol at 5 mg/mL) was utilized for manufacturing nanoASR396 (Avanti Polar Lipids) (28). The solvent from the mixture was evaporated under N_2 gas and re-suspended in saline to make a final concentration of 5 mg/mL of nanoASR396. The rehydrated mixture was heated at 60°C for 60 minutes followed by sonication and extrusion through a 100 mm polycarbonate membrane.

2.5 Estimation of ASR396 encapsulation in nanoASR396.

Drug encapsulation efficiency was performed using a filter separation process as described previously (28). ASR396 not encapsulated in the nanoliposomes was separated by centrifugation for 30 minutes using a 10 kDa filter. Drug from the purified nanoASR396 was extracted by nanoparticle destruction through addition of a 1:1 chloroform and methanol solution. Precipitated lipids were removed by centrifugation and the ASR396 concentration was extrapolated from a standard curve using a UV-visible spectrophotometer with a λmax of 254 nm. Percentage of drug encapsulated was estimated as 1.00 -(free drug after filter separation/total drug before separation) X 100. Release kinetics were measured using dialysis through a 25 kDa membrane. Briefly, nanoASR396 was placed in a dialysis membrane and suspended in 1 L of a saline solution with constant stirring at 300 rpm for 120 hours. A 1-mL sample was taken from the from the dialysis bag at indicated time points, and the concentration of ASR396 was measured by absorption at 254 nm after extracting with 1:1 chloroform: methanol.

2.6 Stability of nanoASR396.

Stability of the nanoliposomes containing ASR396 was performed as described previously (28). NanoASR396 was stored at 4°C for indicated times. The size and charge of the nanoliposomes were calculated using a Malvern Zetasizer. NanoASR396 were considered stable if there was less than a 5% change in the size and charge of the nanoliposomes.

2.7 Confirmation of nanoASR396 structure and size by Cryo-electron microscopy (cryo-EM).

For vitrification, each TEM grid (QUANTIFOIL R 2/1, Electron Microscopy Sciences) with a thin layer of carbon film deposited over the holes was pre-treated by glow discharge. Samples (3.5 μl) were applied to the grid and vitrified using the vitrobot (Thermo Fisher) under the following condition: 4°C, 100% of humidity, and 3 sec of blot time. Images were recorded by the electron microscope Arctica (Thermo Fisher) equipped with Ceta camera (4096 × 4096 pixels, Thermo Fisher). The imaging condition was 92,000X in magnification, 4 in spot size, 2.7 mm in spherical aberration, at an accelerating voltage of 200 KV.

2.8 Assessment of 15-day repeated dose toxicity of nanoASR396.

Swiss-Webster mice were treated intravenously at indicated doses of nanoASR396 daily for 15-days and compared to control nanoliposomes lacking the agent. Changes in the animal body weights, motility and behavioral changes were monitored daily to measure body weight or behavioral related toxic effects (28). At the end of the 15-day treatment regimen, animals were euthanized and blood was collected to assess potential toxic effects. Serum samples were analyzed for levels of biomarkers that correspond to major organ functions as an assessment of toxic effects. Specifically, alanine aminotransferase, alkaline phosphatase, albumin, globulin, total protein, total bilirubin, blood urea nitrogen, glucose, creatinine, calcium and cholesterol were evaluated (29). Levels were compared to animals treated with nanoliposomes lacking ASR396, which served as the control.

2.9 Cell lines, culture conditions and chemicals added to cell culture models.

The human melanoma cell lines, A375M-GFP, UACC 903M-GFP and 1205 Lu-GFP were maintained in DMEM (Invitrogen) supplemented with 5% FBS (Atlantic Biologicals) and GlutaMAX (Life Technologies). Human umbilical vein endothelial cells (HUVEC) were obtained from Lonza and maintained on gelatin-coated plates in endothelial growth media (EGM) supplemented with 2% FBS (Lonza). HEK293A-S1P1-GFP cells were provided by Dr. Tom Kirchhausen (Harvard Medical School) and maintained in DMEM with 10% FBS and 200 μg/ml G418 (30). Melanoma cells were used within 20 passages; HUVEC cells were used between passages 2–5. SEW2871 was purchased from Cayman Chemical and W146 was from TOCRIS. Bradykinin (BK) was obtained from Millipore Sigma and vascular endothelial growth factor (VEGF) and interleukin-8 (IL-8) were from Peprotech.

2.10 HUVEC cell line monolayer model to assess gap formation.

HUVECs were seeded on coverslips coated with fibronectin (Millipore Sigma) and cultured to confluency. The inhibitors of VEGF (Nintedanib), ICAM-1 (A286982), PDE-4(Roflumilast), and mTOR (Tacrolimus), and S1PR1 agonists, SEW2871 (DMSO final concentration: 0.05%), ASR396 (DMSO final concentration: 0.05%) and nanoASR396 (saline) were added to HUVECs at 5 μM for 30 minutes before cells were stimulated with 0.5 μM BK for 30 minutes, 100 ng/mL VEGF or 150 ng/mL IL-8 for 1 hour. HUVECs fixed with 2% cold paraformaldehyde (Electron Microscopy Science) and treated with 0.1% triton X-100 (Fisher) were exposed to a human VE-cadherin antibody (Santa Cruz) followed by the secondary antibody conjugated with Alexa488 (Invitrogen). Coverslips were mounted to slides using the antifade mounting medium with DAPI (Vector Laboratories).

2.11 S1PR1 internalization assay.

HEK293A-S1P1-GFP cells were plated on collagen-coated coverslips (30). Cells were cultured overnight in DMEM with 2% charcoal-stripped serum. Prior to the experiment, cells were cultured in serum-free DMEM for 1.5 hours. Cells were treated with 5 μM W146 for 30 minutes followed by 5 μM SEW2871 and ASR396. After washing with ice cold PBS, cells were fixed in 2% cold paraformaldehyde and mounted to slides using the antifade mounting medium with DAPI.

2.12 Quantitative measurements of permeability coefficient, hydraulic conductivity (Lp) in individually perfused rat mesenteric microvessels.

All animal experimentation in rats was approved by the Animal Care and Use Committee of Pennsylvania State University and met National Institutes of Health standards as set forth in the “Guide for the Care and Use of Laboratory Animals”. Experiments were undertaken on mesenteric venules from female Sprague-Dawley rats (2–3-month old, 220–250 g body weight, Sage Laboratory). Inactin hydrate was used for anesthesia through subcutaneous administration. The initial dosage of inactin was 180 mg/kg body weight and an additional 5 mg/dose given as needed. After the rat reached the appropriate plane of anesthesia, determined by the loss of the toe pinch response and the righting reflex, a midline surgical incision was made in the abdominal wall. A loop of the ileum was gently extended from the abdominal cavity and the mesentery was spread over a pillar attached to an animal tray. The

upper surface of the mesentery was continuously perfused with mammalian Ringer's solution at 37°C. All experiments were carried out on venules with diameters ranging between 40 to 45 μm. Each experiment was performed on a single vessel with one experiment per animal. Euthanasia was performed through bilateral thoracotomy while animals were under anesthesia.

Microvessel permeability was assessed by measuring one of the permeability coefficients, hydraulic conductivity, Lp, using the modified Landis technique. The assumptions and limitations of the method have been evaluated in detail (31–33). Briefly, a single venular microvessel was cannulated with a glass micropipette and perfused with albumin-Ringer solution (control) containing 1% (v/v) rat red blood cells as markers. A hydrostatic pressure (range 40–70 cm H_2O), controlled by a water manometer, was applied through the micropipette to the microvessel lumen. The initial water flux (Jv) per unit area of microvessel wall (S), $(Jv/S)_0$, was calculated from the velocity of the marker cell after the vessel was occluded, the vessel radius, and the length between the marker cell and the occlusion site. Microvessel Lp was calculated from the Starling equation, $Lp = (Jv/S)/\Delta P$, where ΔP represents the pressure difference between the hydrostatic pressure applied to the microvessel and the effective oncotic pressure generated from the albumin in the perfusate, assuming the tissue hydrostatic and oncotic pressures are negligible (31). In each experiment, baseline Lp and the stimulus-induced Lp changes were measured in the same vessel, which allows the changes to be compared with its own control. If Lp is relatively constant throughout the time course, the mean Lp value for each perfusate was calculated from all of the occlusions during that perfusion period. If a transient increase in Lp is observed, Lp is reported as the means of peak and sustained values. Details are shown in Supplementary Figure 1.

2.13 Assessment of off-target effects mediated by nanoASR396 on key signaling pathways using Western blotting.

A monolayer of HUVEC cells following varying treatments were lyzed in RIPA buffer containing protease and phosphatase inhibitors (Pierce Biotechnologies). 20 μg of cell lysate was used for western blotting and probed with antibodies according to the suppliers' recommendations to assess of target effects on several major signaling pathways. Antibodies to p-ERK, ERK, p-PI3K, PI3K, p-FAK, FAK, p-PAK1, PAK1, p-PAK2, PAK2, p-MLC, p-NF-κB, NF-κB were used to probe western blots (Cell Signaling). α Tubulin (Millipore Sigma) was used as a loading control.

2.14 Assessing efficacy of nanoASR396 for inhibiting experimental metastasis.

Animal experimentation in mice was approved by the Animal Care and Use Committee of Pennsylvania State University and met National Institutes of Health standards as set forth in the "Guide for the Care and Use of Laboratory Animals". Athymic $Foxn1^{nu}$ nude mice were intravenously injected with 15 mg/kg nanoASR396 or nanoliposome lacking the agent; (Lipo) vehicle control, for 6, 12 or 18 hours prior to intravenous injection of 1 million A375M-GFP cells in the tail vein. For control comparison purposes, groups of nude mice were injected with 5 mg/kg SEW2871 or DMSO control intraperitoneally. For experiments using UACC 903M-GFP and 1205 Lu-GFP cells, 15 mg/kg nanoASR396 were given 6

hours before cancer cell injection. Body weight was monitored to ensure no significant toxicity during the experimental metastasis assay. On day 29, whole lungs were removed and imaged by fluorescent microscopy to quantify the numbers of metastatic nodules in a double-blinded manner.

2.15 Statistical analysis.

All values of Lp and tumor metastasis were means ± SE. *In vitro* results were shown as mean ± SD. Paired t-test (Nonparametric Wilcoxon matched-paired signed rank test, two-tailed) was used for paired experiments conducted in the same vessel, and Mann-Whitney test (two-tailed) was used for data comparison between two groups. One- and two-way ANOVA with Tukey post hoc test was used to compare data among multiple groups. A probability value of $P < 0.05$ was considered statistically significant. Each "n" of microvessel perfusion experiment represents one experiment conducted in each rat.

3. Results

3.1 Rational for the development of ASR396 off of the chemical structure of SEW2871.

To select the best drug to target endothelial permeability, several anti-inflammatory drugs, including inhibitors of VEGF, ICAM-1, PDE-4 and mTOR and S1PR1 agonists were tested in an *in vitro* endothelial monolayer model and the agents' effects for inhibiting bradykinin (BK)-induced permeability were measured (Supplementary Fig. 2). Most of the anti-inflammatory drugs did not affect the gap formation induced by BK and only S1PR1 agonists reduced the endothelial gap formation in this setting (Supplementary Fig. 2). Since only the activation of S1PR1 inhibits inflammatory mediator-induced increases in microvessel permeability (22), the objective was to make functional group alterations to optimize the structure of S1PR1 agonist SEW2871 (Fig. 1A **left**) for enhanced hydrophilicity; and to make the compound loadable into a nanoliposome without changing its S1PR1 binding activity. A series of derivative SEW2871 compounds (Fig. 1A) were initially proposed that could bind to S1PR1 (Supplementary Table 1). Compound ASR396 (Fig. 1A) was selected from the *in silico* screen because it had a docking score of - 6.278 compared to −2.948 for SEW2871. This occurred because the hydrophobic $–CF_3$ on the phenyl ring of SEW2871 was replaced with a hydrophilic –OH group, which was predicted to enhance its aqueous solubility, potentially facilitating loading into a nanoliposomal formulation.

3.2 Synthesis of ASR396.

SEW2871 derivative ASR396 was then synthesized as shown in Figure 1B. 4-Phenyl-5-trifluoromethyl-thiophene-2-carboxylic acid (1) was first converted *in situ* to the corresponding acid chloride by treating with oxalyl chloride in the presence of catalytic *N,N*-dimethyl formamide. The resulting thiophene carboxylic acid chloride was further reacted with *N*-hydroxy-3-methoxy-benzamidine (2) in the presence of pyridine in xylenes at 140°C for 1 hour yielded the corresponding oxadiazole derivative **3** at a yield of 75% (34). The methoxy compound **3** on further treatment with BCl_3 in CH_2Cl_2 at room temperature for 12 hours resulted in the corresponding hydroxy compound ASR396 at a yield of 92% (Fig. 1B) (35). The structures of compounds **3** and ASR396 were characterized on the basis

of NMR and mass spectral data. No significant change in the binding affinity of ASR396 and SEW2871 to S1PR1 was demonstrated using an S1P1 GPCR cell-based agonist arrestin biosensor assays (Eurofins DiscoverX). SEW2871 and ASR396 showed similar S1PR1 binding kinetics (Fig. 1C) with the EC_{50} of 32 and 43 nM respectively, which suggested no change in binding due to the chemical modification.

3.3 *In silico* predicted off-target binding of ASR396 compared to SEW2871.

To predict whether the chemical modifications of SEW2871 resulting in ASR396 led to any unexpected off-target interactions, the interaction plot of ASR396 with S1PR1 was undertaken. This suggested that the binding scaffold of S1PR1 populated with R120, M124, F125, and V194 had significant interactions with ASR396. R120 and F125 have been reported to be important for maintaining the potency of SEW2871 (36). Hence, the side chain atoms of R120, M124, F125, and V194 engulfing ASR396 in the binding pocket of S1PR1 were extracted and submitted as a query to Erebus. To precisely identify the most similar binding scaffolds to our query structure, a cut-off of RMSD<= 5Å to the query was imposed (Supplementary Table 2). Erebus identified the query substructure itself from S1PR1 in the RCSB database (PDB IDs: 3V2Y, 3V2W) (Supplementary Fig. 3A), which highlights the accuracy of the Erebus algorithm. Further, Erebus identified only one similar rigid binding scaffold, which was soluble epoxide hydrolase (PDB IDs: 3WKE, 3ANT) from *homo sapiens* with RMSDs 3.83 and 4.98, respectively for two structures (Supplementary Fig. 3B). To test whether the identified structural scaffold from soluble epoxide hydrolase had any binding affinity toward ASR396, ASR396 was docked to the predicted site in epoxide hydrolase (PDB ID: 3WKE) using the MedusaDock suite, which is known for its rapid sampling efficiency and high prediction accuracy (37). The docked epoxide hydrolase–ASR396 complex obtained from MedusaDock displayed strong interaction with ASR396 in the Erebus predicted binding scaffold (Supplementary Fig. 3C), which suggested off-target binding to ASR396. Given that the binding of ASR396 to epoxide hydrolase is competitive with the native ligand, the physiological effect may not be pronounced due to strong binding of the endogenous epoxides to epoxide hydrolase (Supplementary Table 3). Apart from these scaffolds, Erebus also identified similar structural scaffolds in proteins from microbial organisms *Geobacillus thermoglucosidasius* and *Peptoclostridium difficile*, which were omitted from the off-targets list since they were not mammalian.

3.4 Development and physiochemical characterization of the nanoliposomal formulation containing ASR396.

To identify a nanoliposomal formulation enabling optimal loading of ASR396, several formulations were examined and results for size, zeta potential charge, membrane potential and surface hydration were evaluated (data not shown). The optimal liposomal formulation selected contained the PEGylated nanoliposomal formulation made of 80:20 mol% ePC: DPPE PEG-2000 called nanoASR396. The average size of the nanoliposomes in saline was 68.14 ± 4.42 nm with a zeta potential charge of 0.24 ± 0.02 mV. Cryo-electron microscopy demonstrated the spherical structure of the nanoliposmes and that the nanoparticles were not aggregations (Fig. 2A). Free ASR396 was solubilized during nanoliposome preparation; however, a small amount of the drug was predicted to be loosely bound to the outer lipid layer of the nanoliposome. The amount of drug in the lipid shell was measured using the

absorption maxima of the drug extrapolated from a standard curve generated from ASR396 ranging from 0.01 and 0.1 mg/ml. The encapsulation efficiency for nanoASR396 after filtration was 67.1% compared to nanoASR396 concentration without extrusion (Fig. 2B).

The drug release kinetics of ASR396 was measured by dialyzing nanoASR396 in saline over 120 hours, upon which the dialyzed nanoliposomes were lysed and the remaining drug measured by extrapolation off a standard curve (Fig. 2C). ASR396 was released from the nanoliposomes at a steady rate over 120 hours with approximately 70 to 75 % release at 72 to 120 hours (Fig. 2C). The stability of refrigerated nanoASR396 was examined weekly for a period of 6 weeks. Size and charge of the nanoASR396 were estimated once every week. Both size (Fig. 2D) and charge (Fig. 2E) of nanoASR396 did not significantly vary over 6 weeks, indicating stability of the formulation. In order to evaluate the safety of the nanoASR396 in animal models, a 14-day repeated range finder study was performed from 15–50 mg/kg intravenously administered daily. Treatment with nanoASR396 did not cause any significant change in animal weight (Fig. 2F) or changes in blood-based biomarkers of major organ related toxicity (Fig. 2G). Hence, nanoASR396 appeared to be a bioavailable agent with potential use in animals.

3.5 NanoASR396 attenuated inflammatory mediator-induced increases in microvessel permeability by activation of endothelial S1PR1.

Previous studies conducted in individually perfused intact microvessels demonstrated that S1P had a potent inhibitory effect on inflammatory mediator-induced increases in microvessel permeability, mediated through the activation of S1PR1 (22,38). In this study, the effect and specificity of the S1PR1 agonist nanoASR396 was examined on platelet activating factor (PAF)-induced permeability increases and results were compared to SEW2871 under the same experimental conditions. Permeability was assessed by measuring hydraulic conductivity, Lp, in individually perfused intact rat mesenteric venules. Each vessel was first cannulated and perfused with the control perfusate (1% bovine serum albumin, BSA, in Ringer's solution) to measure baseline Lp. The mean baseline Lp of 6 vessels was $1.14 \pm 0.16 \times 10^{-7}$ cm/s/cmH_2O. Perfusion of vessels with SEW2871 (10 μM) for 30 minutes did not change the baseline Lp. However, when each of the vessels was perfused with PAF (10 nM) in the presence of SEW2871, the PAF-induced Lp increase was significantly inhibited with the mean Lp value at 1.73 ± 0.15 times that of the control. To test the vessel normal response to PAF, each vessel was given a second application of PAF after washing out SEW2871 with albumin-Ringer perfusion for 40 minutes. Then each vessel showed a typical PAF response with the mean peak Lp increased to 7.50 ± 0.63 times that of the baseline. The time course of the Lp changes from an individual experiment was shown in Figure 3A and the results summary was shown in Figure 3B (n = 6). These results indicated that pre-perfusion of vessels with SEW2871 prevented PAF-induced increases in microvessel Lp, functioning in a similar manner as S1P (22,38).

The effect of nanoASR396 on PAF-induced permeability increases were examined following the same experimental procedures as those used for SEW2871. The mean baseline Lp of 4 vessels was $1.72 \pm 0.13 \times 10^{-7}$ cm/s/cmH_2O. Perfusion of nanoASR396 (100 μM) did not alter baseline Lp but significantly inhibited PAF-induced Lp increase with a mean peak Lp at

2.92 ± 0.14 times that of the control value. In contrast, perfusion of empty nanoliposome alone showed no effect on PAF-induced Lp increase. Overlay of two-individual experiments with the application of nanoASR396 and nanoliposome alone demonstrated that the significant inhibition of PAF-induced Lp increase was due to the effect of ASR396 and not empty nanoliposome (Fig. 4A).

The action of nanoASR396 as a specific S1PR1 agonist was examined in vessels that were pretreated with S1PR1 antagonist W146 before the application of nanoASR396 and PAF. Inhibition of S1PR1 with W146 (10 μM) abolished the effect of nanoASR396 on PAF-induced Lp increases. In four W146-pretreated vessels, the PAF-induced mean peak Lp in the presence of nanoASR396 was 7.12 ± 1.41 times that of the control; insignificant from the Lp responses to PAF in the absence of nanoASR396. Figure 4B shows the time courses of the Lp changes in the absence and presence of W146 from two individual experiments. The summary results of three groups of studies were presented in Figure 4C (n = 4 per group).

3.6 NanoASR396 inhibited endothelial gap formation mediated by inflammatory factors as effectively as SEW2871 acting through the myosin light chain pathway.

The effect of ASR396 on endothelial permeability was further confirmed using a cultured EC monolayer model. As reported by other groups and shown in Figure 5A, vehicle treated ECs in this model had a continuous VE-cadherin junctional protein line between ECs. When treated with vascular endothelial growth factor (VEGF), ECs dissociated from each other to form gaps with a discontinuous distribution line of VE-cadherin (Fig. 5A). ASR396 treatment alone showed a similar result to that observed with the vehicle treated control (Fig. 5A). ECs when treated with both ASR396 and VEGF showed no gap formation with an intact VE-cadherin line at junctions between ECs (Fig. 5A). Quantitation of the gap formation mediated by VEGF (Fig. 5B), demonstrated that ASR396 had similar gap inhibitory efficacy to SEW2871.

ASR396 efficacy for inhibiting gap formation by inflammatory mediators, bradykinin (BK) and interlukin-8 (IL-8) was also examined (Figs. 5A, C and D). As predicted, ECs treated with BK (Fig. 5A), and IL-8 (Fig. 5A) had increased numbers of gaps, while treatment with either ASR396 or SEW2871 similarly inhibited this effect (Figs. 5C, D and E). Thus, ASR396 and SEW2871 similarly blocked gap formation suggesting that ASR396 retained the functional activity of the parent compound.

To show that ASR396 was activating the S1PR1 to prevent gap formation, HUVECs were treated with W146 (S1PR1 antagonist) before treatment with ASR396 and BK. W146 pre-treatment abolished the inhibitory effect of ASR396 on BK-induced gap formation (Fig. 5E), suggesting that ASR396-mediated activation of S1PR1 was responsible for inhibiting gap formation in the EC layer.

A S1PR1 internalization assay using the HEK293A-S1P1-GFP cells was undertaken to show that ASR396 and SEW2871 similarly enhanced S1PR1 internalization, leading to its accumulation in the cytoplasm. Approximately 37% of cells in the DMSO treatment had internalized S1PR1 while more that 75% of cells in the ASR396 (Fig. 5F) and SEW2871

(Fig. 5G) treatment had internalized S1PR1 in the cytoplasm. Internalization mediated by ASR396 and SEW2871 could be blocked using the S1PR1 antagonist W146, suggesting efficacy of both agonists for activating S1PR1 (Figs. 5F and G).

MLC phosphorylation is critical in inducing endothelial barrier permeability (18). HUVECs were treated with BK, VEGF or IL-8 and pMLC levels were compared by western blotting to treatment with ASR396. ASR396 treatment alone did not increase pMLC levels but treatments of BK, VEGF, and IL-8 significantly increased pMLC levels (Fig. 5H). ASR396 was able to reverse and decrease the pMLC levels suggesting that the gap formation was involved in the MLC signaling and reversal effect of ASR396.

NanoASR396 was able to inhibit gap formation mediated by inflammatory mediators VEGF (Fig. 5I), BK (Fig. 5J) and IL-8 (Fig. 5K), compared to EL, similar to that observed with ASR396 in DMSO. No significant difference was observed in EC gap formation between HUVECs treated with ASR396 or nanoASR396 prior to BK, VEGF, and IL-8 exposure. At the concentration of 5 μM, SEW2871, ASR396 and nanoASR396 showed similar potencies to inhibit gap formation Thus, the nanoliposomal lipid formulation did not affect the activity of the compound.

To determine whether ASR396 induced off-target effects in HUVEC cells, the effects of the compound were examined on several signaling pathways important in melanoma development, including the MAPK/ERK, PI3K/AKT, NF-κB, and the vascular permeability regulation pathways. No significant changes in levels or activity of biomarker proteins in these pathways were detected between the control and the ASR396-treated ECs (Supplementary Fig. 4) suggesting that ASR396 did not trigger significant off-target effects.

3.7 NanoASR396 inhibits metastasis similar to that occurring with control SEW2871.

To test the efficacy of nanoASR396 for inhibiting melanoma metastasis, an experimental metastasis mouse model was used and the treatment protocol summarized in Fig. 6A. Mice were treated with nanoASR396 intravenously prior to injecting GFP-tagged A375M, UACC 903M or 1205 Lu melanoma cells. Control mice for the A375M cell line developed 45 visible A375M-GFP melanoma metastatic nodules in the lung while mice treated with with nanoASR396 developed only 9–16 metastatic nodules, which was an 65–80% reduction (Fig. 6B). NanoASR396 treatment also led to a 62.7% reduction in UACC 903M-GFP (Fig. 6C) and 79.1% reduction in 1205 Lu-GFP (Fig. 6D) melanoma cell-mediated metastasis confirming this efficacy. To compare the effects of nanoASR396 to SEW2871 on metastasis inhibition, mice were treated with SEW2871 intraperitoneally before the administration of A375M-GFP melanoma cells. Control mice developed 62 visible A375M-GFP melanoma metastatic nodules in the lungs, while mice treated with SEW2871 developed 17–27 metastatic nodules (Fig. 6E). Thus, mice treated with nanoASR396 had melanoma metastasis in the lung reduced up to 80%, which was similar to that observed with SEW2871, suggesting it could be a potentially effective metastasis inhibitor.

4. Discussion

S1P can potently inhibit inflammatory mediator-induced increases in microvessel permeability through the activation of S1PR1 (22,38). Based on those observations, we developed a new nanoparticle based S1PR1 agonist, called nanoASR396, to specifically reverse the cancer-associated vascular inflammation that promotes metastasis. Studies conducted in both intact microvessels and a cultured EC monolayer model demonstrated its potent efficacy for enhancing endothelial barrier integrity, function, inhibition of permeability increases, and EC gap formation mediated by a variety of inflammatory mediators as well as tumor cell secreted cytokines. Significantly, the effect of S1PR1 agonist nanoASR396 inhibited the inflammatory mediator-induced permeability increases using a quantitative measure of the permeability coefficient, Lp, in intact rat microvessels. NanoASR396 inhibited PAF-induced permeability increases similar to that observed with the SEW2871 control. Furthermore, the action of nanoASR396 was abolished by pretreating vessels with a S1PR1 antagonist, W146, which confirmed the effect of nanoASR396 occurred through S1PR1 activation in ECs. Most importantly, systemic application of nanoASR396 inhibited lung metastasis by up to 80% in a melanoma metastasis animal model. Results demonstrated that the action of nanoASR396 not only recapitulated the effect of S1P on EC barrier integrity, but also minimized the potential confounding effects of S1P on the activation of other S1P receptors, suggesting its clinical potential for retarding the metastatic spread of cancer.

ASR396 was developed from SEW2871, which can be loaded into a nanoliposome for bioavailable intravenous delivery. The chemical structure of ASR396 was found to have better binding interaction in the S1PR1 active pocket with a higher docking score compared to SEW2871. ASR396 was also confirmed to specifically interact in the active pocket of S1PR1 using the Erebus algorithm. Binding of ASR396 to S1PR1 and activation of S1PR1 was found to be similar to SEW2871. The binding of ASR396 to S1PR1 could be blocked using the S1PR1 antagonist W146 (like SEW2871), which functionally demonstrated that the new compound maintained its binding to the receptor. Thus, the data suggested that ASR396 was a specific S1PR1 agonist, functioning like SEW2871.

VEGF, BK and IL-8 are some of the inflammatory cytokines that are elevated in the serum of advanced-stage melanoma patients and in animal models containing melanomas (13). These cytokines can significantly alter the architecture of VE-cadherin and the phosphorylation status of MLC in endothelial cells leading to the detachment of these cells from one another to form gaps (45,46). VEGF and BK are well-known permeability inducers and mechanisms mediating this process has been reviewed in detail (47). The IL-8 and CXCR1/2 complex has been shown to increase vascular permeability by transactivating VEGFR2 (48). It is almost impossible to target each individual inflammatory cytokine in order to prevent their effects on EC integrity. Therefore, our approach of directly enhancing the EC barrier integrity to prevent gap formation-mediated by a wide-spectrum of inflammatory cytokines could effectively reduce cancer cell metastasis for many cancer types and not just melanoma.

A major advantage of ASR396 is that it can be encapsulated into nanoliposomes while SEW2871 cannot. In recent years, nanotechnology has been used to more effectively deliver agents to treat cancer by reducing toxicity, increasing bioavailability and prolonging the time in the circulation (53). Nanoparticles can increase drug solubility, improve pharmacokinetics and minimize side-effects (53). Nanoliposomes, compared to the traditional drug delivery route, have some promising benefits, including better drug delivery, protection of active drugs from environmental factors, prevention of early degradation of the drug, cost-effective formulation for expensive agents and more efficient treatments with less toxicity (54). Moreover, the biodegradability and biocompatibility of nanoliposomes make them excellent therapeutic vehicles (53). Using a melanoma mouse model, our group has demonstrated the low toxicity, high bioavailability and prolonged release of the nanoliposomal forms of anti-melanoma drugs, such as leelamine (55), arachidonyl trifluoromethyl ketone (56), aldehyde dehyrdrogenase inhibitors (57), celecoxib (58), and plumbagin (58).

NanoASR396 increased bioavailability by enabling direct injection into the vascular system where it would have immediate access to the ECs where it needed to act. NanoASR396 inhibited EC gap formation in the vascular system, which led to fewer melanoma lung metastases. We have previously shown that melanoma cells secrete IL-8 to attract neutrophils which tether them to the vascular endothelial cell layer to promote metastasis (59). The results of this study extend this process by showing that the cytokines secreted by these cells can further aid this process by enabling gap formation in the EC layer through which the cancer cells can extravasate to promote metastasis. This process can be inhibited using the bioavailable nanoASR396, which releases the S1PR1 agonist at the EC layer to enhance vascular barrier integrity. Thus, it is possible to counteract the effects of inflammatory cytokines non-specifically and provide better protection against these factors to maintain EC homeostasis to inhibit inflammation-mediated melanoma metastasis.

In normal endothelial cells, the S1P/S1PR1 complex enhances junctional assembly (49) while at high concentration of S1P, the S1P/S1PR3 complex in endothelial cells disrupts the barrier structure (50). An S1PR1/3 agonist, FTY720, has been developed but has the side-effects of inducing bradycardia (51), macular oedema, cardiovascular complications, and brain inflammation(52). This occurs following the activation of S1PR3 (51) or S1PR1 and S1PR3 (52). Since ASR396 is a specific agonist to S1PR1, these toxic effects would not likely be observed.

S1P through the S1P receptors has been reported to trigger a possible epithelial-to-mesenchymal transition (EMT), leading to increased cell migration, invasion and metastasis in breast, liver and melanoma (39–41). In melanoma, the main S1P receptor regulating the S1P-mediated EMT and cell invasion has been reported to be S1PR3 (39), therefore, using the specific S1PR1 agonist nanoASR396 would likely avoid this concern. The S1PR1 pathway has been reported to be involved in S1P-mediated lymphangiogenesis, which indicates a potential role in lymphatic cancer metastasis (42). A recent study showed that S1PR1 plays a crucial role in high-molecular-weight-hyaluronan-mediated permeability decrease in cancer lymphatic endothelial cell monolayer (43). Effects, if any, of ASR396 on melanoma lymphatic metastasis remain to be examined. However, since surgical cancer excision has potential to disseminate cancer around the patient’s body (44), a single

treatment of nanoASR396 might be sufficient for use prior to melanoma surgery to enhance endothelial cell junctional integrity, in order to reduce surgery-mediated cancer spread. Since this treatment modality would only require a single administration of nanoASR396, this approach could reduce the concerns related to potential EMT-mediated effects occurring with long-term treatment.

In summary, this report suggests that multiple inflammatory cytokines secreted from melanoma cells can create gaps in the EC layer, which can subsequently promote metastasis. To combat vascular endothelial inflammation mediated by these factors, a novel S1PR1 agonist, called ASR396 has been developed, which could reverse the collective effect of these proteins. Compared to SEW2871, ASR396 exhibited several significant advantages including better association with S1PR1 and loadability into a nanoliposome. NanoASR396 had an average size of 69 nm, neutral-charge in saline and was stable for 6 weeks when refrigerated. NanoASR396 significantly prevented permeability increases and gap formation in the vascular endothelium and an EC monolayer model induced by inflammatory cytokines. NanoASR396 enhanced endothelial cell layer integrity by decreasing the phosphorylation of MLC. As a result, melanoma lung metastasis development was inhibited. Endothelial homeostasis plays a key role in metastasis and enhancing the endothelial barrier integrity using the novel bioavailable S1PR1 agonist nanoASR396 was a potentially effective strategy to reduce metastasis.

Supplementary Material

Refer to Web version on PubMed Central for supplementary material.

Acknowledgments

Financial support: G.P.R acknowledges the support of The Foreman Foundation for Melanoma Research, The Mike Geltrude Foundation and Penn State Chocolate Tour Cancer Research Fund. P.H. acknowledges the support of the National Institutes of Health DK097391, HL130363, and HL144620. N.V.D. acknowledges support of the National Institutes of Health grants R01 GM114015 and R35 GM134864, Passan Foundation, and CTSI Bridges to Translation V Pilot Award.

Reference

1. Chaffer CL, Weinberg RA. A perspective on cancer cell metastasis. Science (New York, NY) 2011;331(6024):1559–64 doi 10.1126/science.1203543.
2. Guan X. Cancer metastases: challenges and opportunities. Acta Pharm Sin B 2015;5(5):402–18 doi 10.1016/j.apsb.2015.07.005. [PubMed: 26579471]
3. Seyfried TN, Huysentruyt LC. On the origin of cancer metastasis. Crit Rev Oncog 2013;18(1–2):43–73. [PubMed: 23237552]
4. Zeeshan R, Mutahir Z. Cancer metastasis - tricks of the trade. Bosn J Basic Med Sci 2017;17(3):172–82 doi 10.17305/bjbms.2017.1908. [PubMed: 28278128]
5. Poste G, Fidler IJ. The pathogenesis of cancer metastasis. Nature 1980;283(5743):139–46 doi 10.1038/283139a0. [PubMed: 6985715]
6. Reymond N, d'Agua BB, Ridley AJ. Crossing the endothelial barrier during metastasis. Nature reviews Cancer 2013;13(12):858–70 doi 10.1038/nrc3628. [PubMed: 24263189]
7. Blazejczyk A, Papiernik D, Porshneva K, Sadowska J, Wietrzyk J. Endothelium and cancer metastasis: Perspectives for antimetastatic therapy. Pharmacol Rep 2015;67(4):711–8 doi 10.1016/j.pharep.2015.05.014. [PubMed: 26321272]

8. Frolow M, Drozdz A, Kowalewska A, Nizankowski R, Chlopicki S. Comprehensive assessment of vascular health in patients; towards endothelium-guided therapy. Pharmacol Rep 2015;67(4):786–92 doi 10.1016/j.pharep.2015.05.010. [PubMed: 26321282]
9. Walczak M, Suraj J, Kus K, Kij A, Zakrzewska A, Chlopicki S. Towards a comprehensive endothelial biomarkers profiling and endothelium-guided pharmacotherapy. Pharmacol Rep 2015;67(4):771–7 doi 10.1016/j.pharep.2015.06.008. [PubMed: 26321280]
10. Garcia-Roman J, Zentella-Dehesa A. Vascular permeability changes involved in tumor metastasis. Cancer Lett 2013;335(2):259–69 doi 10.1016/j.canlet.2013.03.005. [PubMed: 23499893]
11. Roblek M, Protsyuk D, Becker PF, Stefanescu C, Gorzelanny C, Glaus Garzon JF, et al. CCL2 Is a Vascular Permeability Factor Inducing CCR2-Dependent Endothelial Retraction during Lung Metastasis. Mol Cancer Res 2019;17(3):783–93 doi 10.1158/1541-7786.MCR-18-0530. [PubMed: 30552233]
12. Weidert E, Pohler SE, Gomez EW, Dong C. Actinomyosin contraction, phosphorylation of VE-cadherin, and actin remodeling enable melanoma-induced endothelial cell-cell junction disassembly. PloS one 2014;9(9):e108092 doi 10.1371/journal.pone.0108092.
13. Yurkovetsky ZR, Kirkwood JM, Edington HD, Marrangoni AM, Velikokhatnaya L, Winans MT, et al. Multiplex analysis of serum cytokines in melanoma patients treated with interferon-alpha2b. Clinical cancer research : an official journal of the American Association for Cancer Research 2007;13(8):2422–8 doi 10.1158/1078-0432.Ccr-06-1805.
14. Zhang P, Feng S, Liu G, Wang H, Zhu H, Ren Q, et al. Mutant B-Raf(V600E) Promotes Melanoma Paracellular Transmigration by Inducing Thrombin-mediated Endothelial Junction Breakdown. The Journal of biological chemistry 2016;291(5):2087–106 doi 10.1074/jbc.M115.696419. [PubMed: 26504080]
15. Wallez Y, Huber P. Endothelial adherens and tight junctions in vascular homeostasis, inflammation and angiogenesis. Biochimica et biophysica acta 2008;1778(3):794–809 doi 10.1016/j.bbamem.2007.09.003. [PubMed: 17961505]
16. Vincent PA, Xiao K, Buckley KM, Kowalczyk AP. VE-cadherin: adhesion at arm's length. American journal of physiology Cell physiology 2004;286(5):C987–97 doi 10.1152/ajpcell.00522.2003. [PubMed: 15075197]
17. Rigor RR, Shen Q, Pivetti CD, Wu MH, Yuan SY. Myosin light chain kinase signaling in endothelial barrier dysfunction. Medicinal research reviews 2013;33(5):911–33 doi 10.1002/med.21270. [PubMed: 22886693]
18. Cai S, Pestic-Dragovich L, O'Donnell ME, Wang N, Ingber D, Elson E, et al. Regulation of cytoskeletal mechanics and cell growth by myosin light chain phosphorylation. The American journal of physiology 1998;275(5):C1349–56 doi 10.1152/ajpcell.1998.275.5.C1349. [PubMed: 9814984]
19. Garcia JG, Davis HW, Patterson CE. Regulation of endothelial cell gap formation and barrier dysfunction: role of myosin light chain phosphorylation. Journal of cellular physiology 1995;163(3):510–22 doi 10.1002/jcp.1041630311. [PubMed: 7775594]
20. Winkler MS, Nierhaus A, Poppe A, Greiwe G, Graler MH, Daum G. Sphingosine-1-Phosphate: A Potential Biomarker and Therapeutic Target for Endothelial Dysfunction and Sepsis? Shock (Augusta, Ga) 2017;47(6):666–72 doi 10.1097/shk.0000000000000814.
21. Xiong Y, Hla T. S1P control of endothelial integrity. Curr Top Microbiol Immunol 2014;378:85–105 doi 10.1007/978-3-319-05879-5_4. [PubMed: 24728594]
22. Zhang G, Xu S, Qian Y, He P. Sphingosine-1-phosphate prevents permeability increases via activation of endothelial sphingosine-1-phosphate receptor 1 in rat venules. American journal of physiology Heart and circulatory physiology 2010;299(5):H1494–504 doi 10.1152/ajpheart.00462.2010. [PubMed: 20729401]
23. Park SJ, Im DS. Sphingosine 1-Phosphate Receptor Modulators and Drug Discovery. Biomolecules & therapeutics 2017;25(1):80–90 doi 10.4062/biomolther.2016.160. [PubMed: 28035084]
24. Sharma S, Mathur AG, Pradhan S, Singh DB, Gupta S. Fingolimod (FTY720): First approved oral therapy for multiple sclerosis. J Pharmacol Pharmacother 2011;2(1):49–51 doi 10.4103/0976-500X.77118. [PubMed: 21701650]

25. Dyckman AJ. Modulators of Sphingosine-1-phosphate Pathway Biology: Recent Advances of Sphingosine-1-phosphate Receptor 1 (S1P1) Agonists and Future Perspectives. Journal of medicinal chemistry 2017;60(13):5267–89 doi 10.1021/acs.jmedchem.6b01575. [PubMed: 28291340]
26. Pulla VK, Sriram DS, Soni V, Viswanadha S, Sriram D, Yogeeswari P. Targeting NAMPT for Therapeutic Intervention in Cancer and Inflammation: Structure-Based Drug Design and Biological Screening. Chem Biol Drug Des 2015;86(4):881–94 doi 10.1111/cbdd.12562. [PubMed: 25850461]
27. Shirvanyants D, Alexandrova AN, Dokholyan NV. Rigid substructure search. Bioinformatics 2011;27(9):1327–9 doi 10.1093/bioinformatics/btr129. [PubMed: 21460026]
28. Gowda R, Dinavahi SS, Iyer S, Banerjee S, Neves RI, Pameijer CR, et al. Nanoliposomal delivery of cytosolic phospholipase A(2) inhibitor arachidonyl trimethyl ketone for melanoma treatment. Nanomedicine 2018;14(3):863–73 doi 10.1016/j.nano.2017.12.020. [PubMed: 29317343]
29. Dinavahi SS, Gowda R, Gowda K, Bazewicz CG, Chirasani VR, Battu MB, et al. Development of a Novel Multi-Isoform ALDH Inhibitor Effective as an Antimelanoma Agent. Molecular cancer therapeutics 2020;19(2):447 doi 10.1158/1535-7163.MCT-19-0360. [PubMed: 31754071]
30. Reeves PM, Kang Y-L, Kirchhausen T. Endocytosis of Ligand-Activated Sphingosine 1-Phosphate Receptor 1 Mediated by the Clathrin-Pathway. Traffic 2016;17(1):40–52 doi 10.1111/tra.12343. [PubMed: 26481905]
31. Kendall S, Michel CC. The measurement of permeability in single rat venules using the red cell microperfusion technique. Experimental physiology 1995;80(3):359–72 doi 10.1113/expphysiol.1995.sp003853. [PubMed: 7640005]
32. Curry FE, Huxley VH, Sarelius IH. Techniques in the microcirculation : measure of permeability, pressure and flow. County Clare, Ireland; New York: Elsevier Scientific Publishers Ireland; Sole distributors for the U.S.A. and Canada, Elsevier Scientific Pub. Co.; 1983.
33. He P, Zhang X, Curry FE. Ca2+ entry through conductive pathway modulates receptor-mediated increase in microvessel permeability. The American journal of physiology 1996;271(6 Pt 2):H2377–87 doi 10.1152/ajpheart.1996.271.6.H2377. [PubMed: 8997296]
34. Hale JJ, Lynch CL, Neway W, Mills SG, Hajdu R, Keohane CA, et al. A rational utilization of high-throughput screening affords selective, orally bioavailable 1-benzyl-3-carboxyazetidine sphingosine-1-phosphate-1 receptor agonists. Journal of medicinal chemistry 2004;47(27):6662–5 doi 10.1021/jm0492507. [PubMed: 15615513]
35. Tanaka M, Ohshima T, Mitsuhashi H, Maruno M, Wakamatsu T. Total syntheses of the lignans isolated from Schisandra Chinensis. Tetrahedron 1995;51(43):11693–702 doi 10.1016/0040-4020(95)00701-9.
36. van Loenen PB, de Graaf C, Verzijl D, Leurs R, Rognan D, Peters SL, et al. Agonist-dependent effects of mutations in the sphingosine-1-phosphate type 1 receptor. European journal of pharmacology 2011;667(1–3):105–12 doi 10.1016/j.ejphar.2011.05.071. [PubMed: 21663738]
37. Ding F, Yin S, Dokholyan NV. Rapid flexible docking using a stochastic rotamer library of ligands. J Chem Inf Model 2010;50(9):1623–32 doi 10.1021/ci100218t. [PubMed: 20712341]
38. Minnear FL, Zhu L, He P. Sphingosine 1-phosphate prevents platelet-activating factor-induced increase in hydraulic conductivity in rat mesenteric venules: pertussis toxin sensitive. American journal of physiology Heart and circulatory physiology 2005;289(2):H840–4 doi 10.1152/ajpheart.00026.2005. [PubMed: 15778280]
39. Albinet V, Bats ML, Huwiler A, Rochaix P, Chevreau C, Segui B, et al. Dual role of sphingosine kinase-1 in promoting the differentiation of dermal fibroblasts and the dissemination of melanoma cells. Oncogene 2014;33(26):3364–73 doi 10.1038/onc.2013.303. [PubMed: 23893239]
40. Kim E-S, Kim J-S, Kim SG, Hwang S, Lee CH, Moon A. Sphingosine 1-phosphate regulates matrix metalloproteinase-9 expression and breast cell invasion through S1P3–Gαq coupling. J Cell Sci 2011;124(13):2220–30 doi 10.1242/jcs.076794. [PubMed: 21652634]
41. Zeng Y, Yao X, Chen L, Yan Z, Liu J, Zhang Y, et al. Sphingosine-1-phosphate induced epithelial-mesenchymal transition of hepatocellular carcinoma via an MMP-7/ syndecan-1/TGF-β autocrine loop. Oncotarget 2016;7(39):63324–37 doi 10.18632/oncotarget.11450. [PubMed: 27556509]

42. Yoon CM, Hong BS, Moon HG, Lim S, Suh P-G, Kim Y-K, et al. Sphingosine-1-phosphate promotes lymphangiogenesis by stimulating S1P1/Gi/PLC/Ca2+ signaling pathways. Blood 2008;112(4):1129–38 doi 10.1182/blood-2007-11-125203. [PubMed: 18541717]
43. Yu M, He P, Liu Y, He Y, Du Y, Wu M, et al. Hyaluroan-regulated lymphatic permeability through S1P receptors is crucial for cancer metastasis. Medical Oncology 2014;32(1):381 doi 10.1007/s12032-014-0381-1. [PubMed: 25428387]
44. Tohme S, Simmons RL, Tsung A. Surgery for Cancer: A Trigger for Metastases. Cancer research 2017;77(7):1548 doi 10.1158/0008-5472.CAN-16-1536. [PubMed: 28330928]
45. Azzi S, Hebda J, GAVARD J. Vascular Permeability and Drug Delivery in Cancers. Frontiers in Oncology 2013;3(211) doi 10.3389/fonc.2013.00211.
46. Giannotta M, Trani M, Dejana E. VE-cadherin and endothelial adherens junctions: active guardians of vascular integrity. Developmental cell 2013;26(5):441–54 doi 10.1016/j.devcel.2013.08.020. [PubMed: 24044891]
47. Mehta D, Malik AB. Signaling mechanisms regulating endothelial permeability. Physiological reviews 2006;86(1):279–367 doi 10.1152/physrev.00012.2005. [PubMed: 16371600]
48. Petreaca ML, Yao M, Liu Y, Defea K, Martins-Green M. Transactivation of vascular endothelial growth factor receptor-2 by interleukin-8 (IL-8/CXCL8) is required for IL-8/CXCL8-induced endothelial permeability. Mol Biol Cell 2007;18(12):5014–23 doi 10.1091/mbc.e07-01-0004. [PubMed: 17928406]
49. Mehta D, Konstantoulaki M, Ahmmed GU, Malik AB. Sphingosine 1-phosphate-induced mobilization of intracellular Ca2+ mediates rac activation and adherens junction assembly in endothelial cells. The Journal of biological chemistry 2005;280(17):17320–8 doi 10.1074/jbc.M411674200. [PubMed: 15728185]
50. Komarova YA, Mehta D, Malik AB. Dual regulation of endothelial junctional permeability. Science's STKE : signal transduction knowledge environment 2007;2007(412):re8 doi 10.1126/stke.4122007re8.
51. Sanna MG, Liao J, Jo E, Alfonso C, Ahn MY, Peterson MS, et al. Sphingosine 1-phosphate (S1P) receptor subtypes S1P1 and S1P3, respectively, regulate lymphocyte recirculation and heart rate. The Journal of biological chemistry 2004;279(14):13839–48 doi 10.1074/jbc.M311743200. [PubMed: 14732717]
52. Takasaki T, Hagihara K, Satoh R, Sugiura R. More than Just an Immunosuppressant: The Emerging Role of FTY720 as a Novel Inducer of ROS and Apoptosis. Oxidative medicine and cellular longevity 2018;2018:4397159 doi 10.1155/2018/4397159.
53. Din FU, Aman W, Ullah I, Qureshi OS, Mustapha O, Shafique S, et al. Effective use of nanocarriers as drug delivery systems for the treatment of selected tumors. International journal of nanomedicine 2017;12:7291–309 doi 10.2147/IJN.S146315. [PubMed: 29042776]
54. Deshpande PP, Biswas S, Torchilin VP. Current trends in the use of liposomes for tumor targeting. Nanomedicine (London, England) 2013;8(9):1509–28 doi 10.2217/nnm.13.118.
55. Chen YC, Gowda R, Newswanger RK, Leibich P, Fell B, Rosenberg G, et al. Targeting cholesterol transport in circulating melanoma cells to inhibit metastasis. Pigment Cell Melanoma Res 2017;30(6):541–52 doi 10.1111/pcmr.12614. [PubMed: 28685959]
56. Gowda R, Dinavahi SS, Iyer S, Banerjee S, Neves RI, Pameijer CR, et al. Nanoliposomal delivery of cytosolic phospholipase A2 inhibitor arachidonyl trimethyl ketone for melanoma treatment. Nanomedicine 2018;14(3):863–73 doi 10.1016/j.nano.2017.12.020. [PubMed: 29317343]
57. Dinavahi SS, Gowda R, Gowda K, Bazewicz CG, Chirasani VR, Battu MB, et al. Development of a novel multi-isoform ALDH inhibitor effective as an anti-melanoma agent. Molecular cancer therapeutics 2019 doi 10.1158/1535-7163.Mct-19-0360.
58. Gowda R, Kardos G, Sharma A, Singh S, Robertson GP. Nanoparticle-Based Celecoxib and Plumbagin for the Synergistic Treatment of Melanoma. Molecular cancer therapeutics 2017;16(3):440–52 doi 10.1158/1535-7163.MCT-16-0285. [PubMed: 28003325]
59. Huh SJ, Liang S, Sharma A, Dong C, Robertson GP. Transiently entrapped circulating tumor cells interact with neutrophils to facilitate lung metastasis development. Cancer research 2010;70(14):6071–82 doi 10.1158/0008-5472.CAN-09-4442. [PubMed: 20610626]

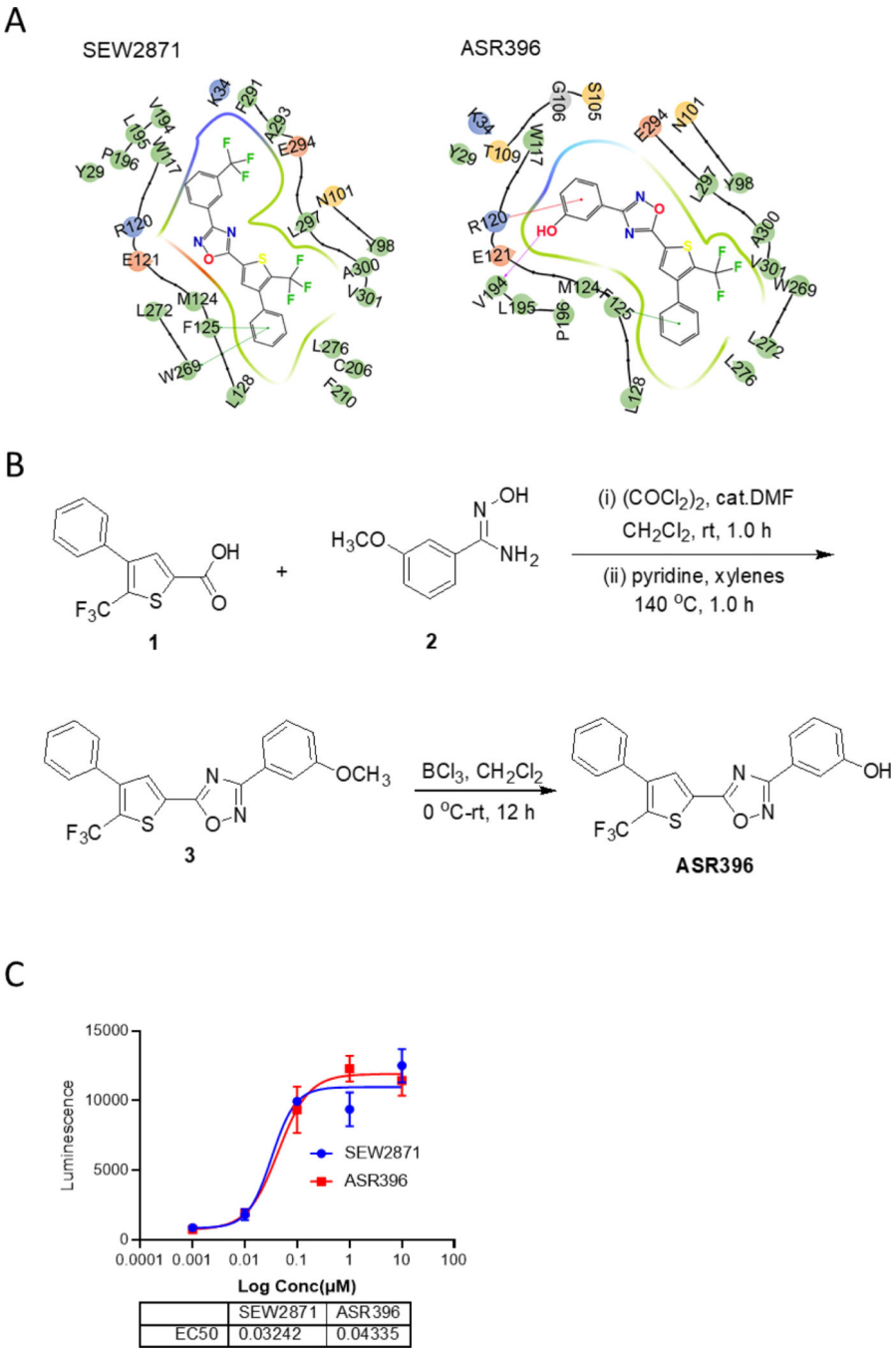

Figure 1. Development of a novel S1PR1 agonist, ASR396.

(A) Docking studies were performed on the active site pocket of S1PR1 to evaluate the binding of SEW2871 and ASR396 compounds. (B) Synthesis scheme for the ASR396 compound. (C) Binding affinity of SEW2871 and ASR396 to S1PR1.

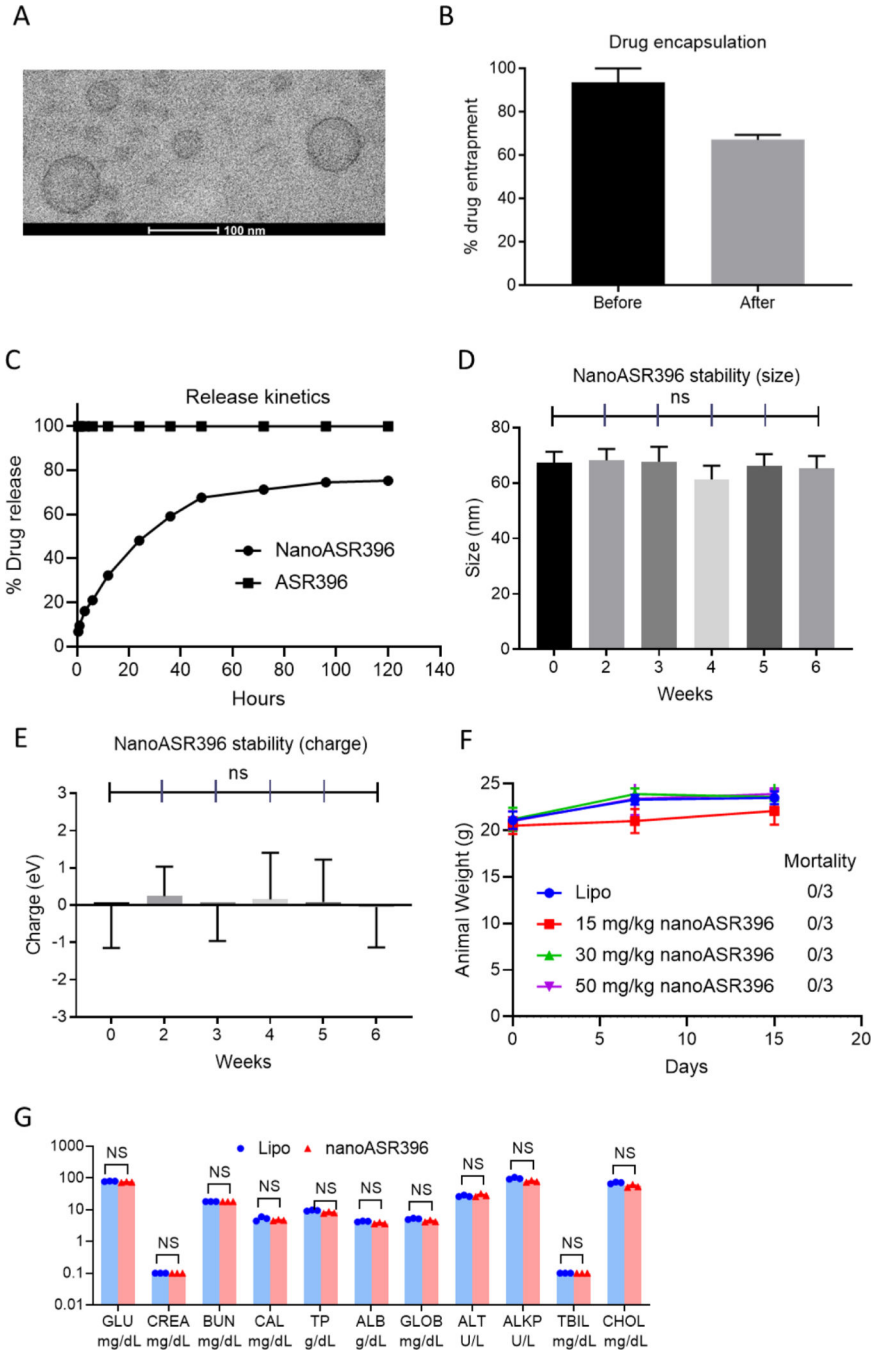

Figure 2. Characterization of NanoASR396.

The nanoliposomal formulation of ASR396 was characterized by: (A) Cryogenic electron microscopy. The size of particles ranged from 10 nm to 80 nm in diameter. Scale bar = 100 nm; (B) drug encapsulation; (C) release kinetics; and, (D&E) stability by examination of size and charge changes over a 6-week period. Drug encapsulation was calculated by estimating the concentration of ASR396 in the nanoliposomes before and after membrane filtration. In-vitro release kinetics were performed using a dialysis in a saline solution. (F) A 15-days of continuous daily treatment with ASR396 nanoliposomes toxicity evaluation of

nanoASR396 demonstrated no toxicity as evidenced through behavioral or weight changes in animals. Treatment did not lead to animal mortality. (G) Assessment of serum biomarkers of major organ functions to determine toxicity, showed no difference between drug compared to vehicle treated animal controls following 15-days of continuous daily treatment with ASR396 nanoliposomes. Empty nanoliposomes (Lipo) served as the control to which ASR396 was compared.

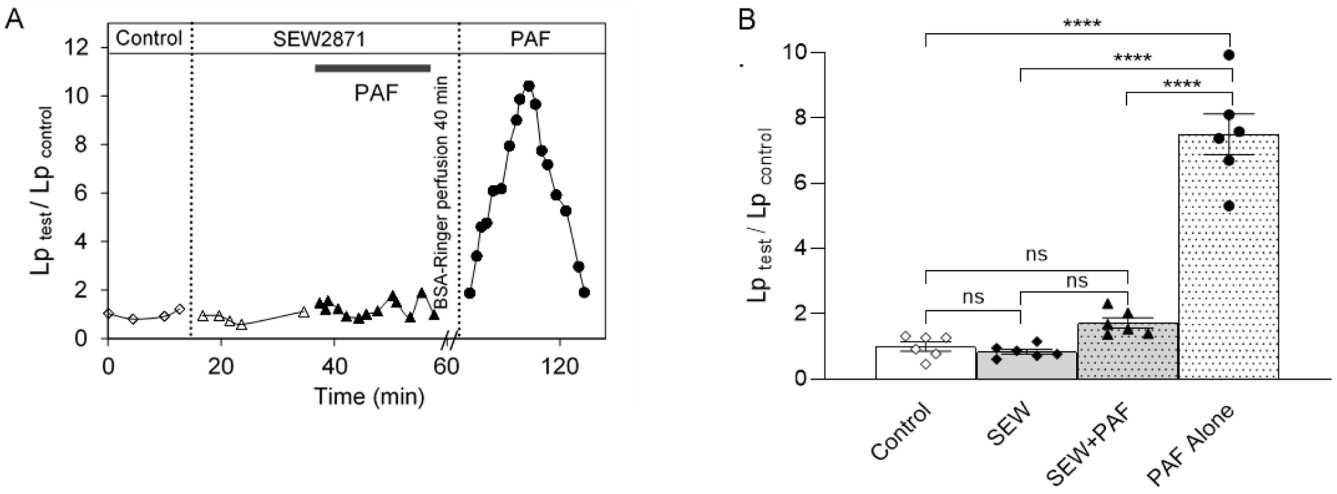

Figure 3. Activation of S1PR1 with agonist SEW2871 significantly attenuated platelet activating factor (PAF)-induced increases in rat microvessel permeability.

Microvessel permeability was assessed by measuring one of the permeability coefficients hydraulic conductivity, Lp, in individually perfused intact rat mesenteric venules. (A) An individual representative experiment shows the time course of the Lp changes measured in the same vessel. (B) Summary results of 6 experiments. Each vessel had control and all treatment measurements as that shown in A, and the Lp changes were compared with its own control. Perfusion of vessels with SEW2871 (SEW, 10 μM) did not alter baseline Lp but significantly inhibited PAF-induced Lp increase. After washing away SEW2871 and PAF with BSA-Ringer perfusion for 40 minutes, each vessel was exposed to a second application of PAF and showed a typical PAF-induced Lp increase, indicating each vessel was responsive to PAF. ns $p \geq 0.23$. **** $p \leq 0.0001$

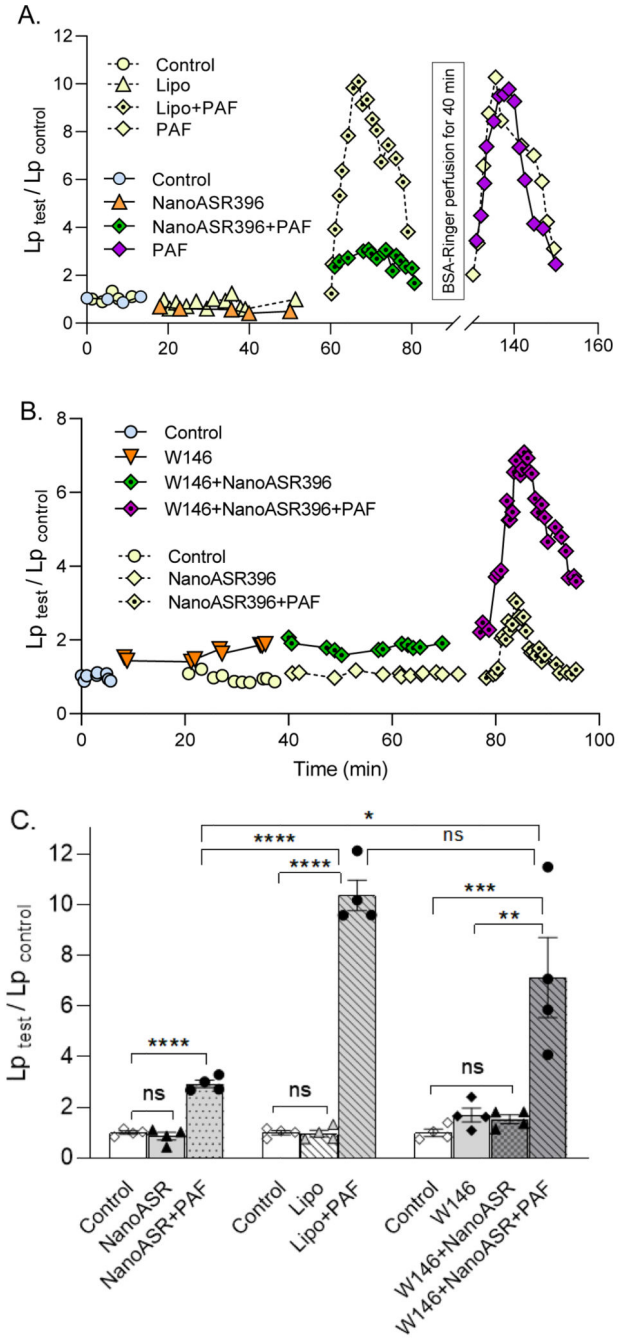

Figure 4. NanoASR396 inhibits PAF-induced permeability increases in intact rat microvessels by activation of endothelial S1PR1.

(A & C) Hydraulic conductivity (Lp) measured in individually perfused intact rat microvessels showed that the application of nanoASR396 (nanoASR, 100 μM) did not alter baseline Lp but significantly attenuated a PAF (10 nM)-induced Lp increase. The perfusion of empty nanoliposome (Lipo) alone showed no such effect. The time courses of the Lp changes from two individual experiments using nanoASR396 and empty nanoliposome alone were overlaid in (A) to show the contrasting effects on PAF-induced Lp increases. When each vessel was exposed to PAF alone for the second time, both vessels responded to

PAF to a similar magnitude, indicating the suppressed Lp response to PAF in the presence of NanoASR396 was due to the inhibitory effect of released ASR396, not variability in vessel response. (B & C) NanoASR396 effect on PAF-induced Lp increase was due to S1PR1 activation on the endothelium. Pre-perfusing vessels with 10 μM W146, an antagonist of S1PR1, abolished the inhibitory effect of nanoASR396 on PAF-induced Lp increase. (B) The overlaid two individual experiments demonstrated the contrast of PAF-induced Lp increase. (C) Results summary. ns $p \geq 0.71$. * $p = 0.038$. ** $p = 0.002$. *** $p = 0.001$. **** $p \leq 0.0001$.

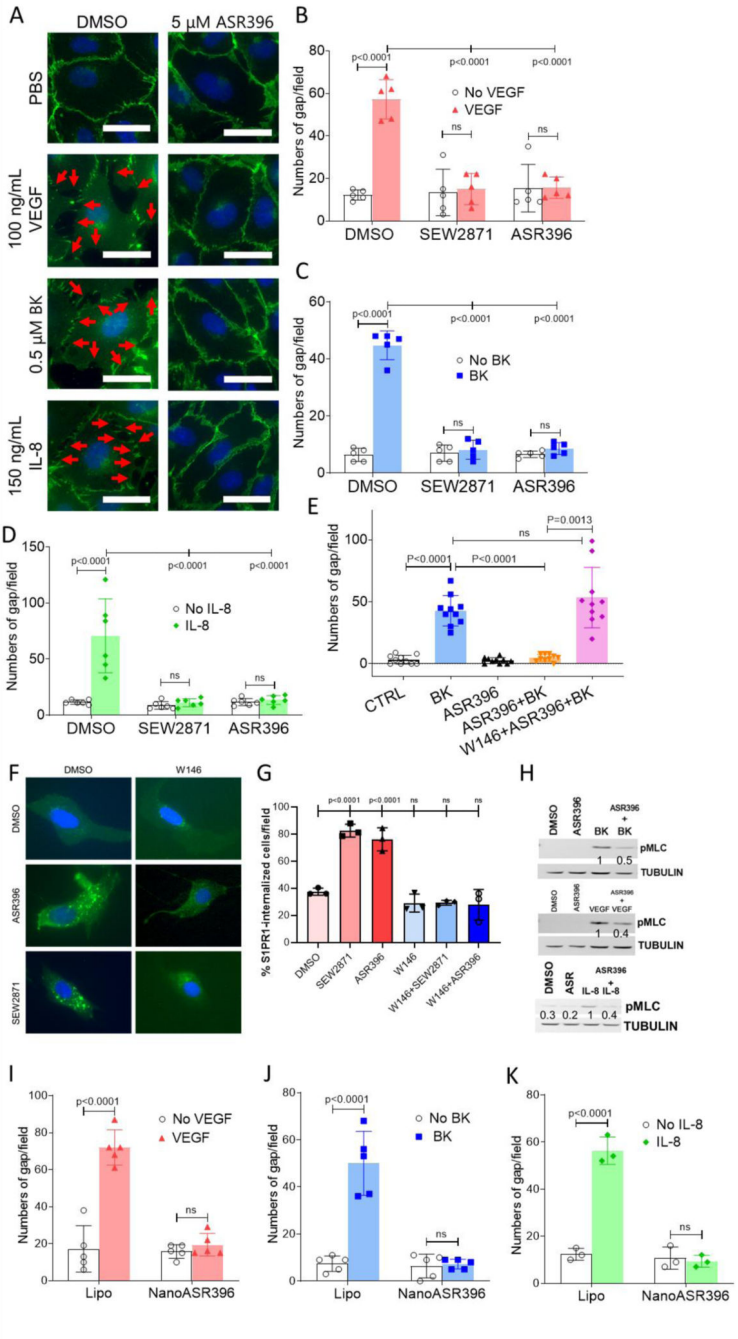

Figure 5. NanoASR396 reverses the effects of inflammatory mediators on the cultured endothelial cell monolayer model.

(A) Representative images showed the VE-cadherin distribution after ASR396, VEGF, BK, IL-8 and the combination of ASR396 plus the inflammatory mediator treatment on ECs in the monolayer EC model. Arrows point to the discontinuous VE-cadherin line at the EC membrane junction, indicating gap formation. Scale bar: 20 μm. (B, C & D) 5 μM SEW2871 and ASR396 reduced the EC gap formation induced by: (B) 100 ng/ml VEGF, (C) 0.5 μM BK and (D) 150 ng/ml IL-8. SEW2871 and ASR396 alone did not affect EC gap formation. (E) 5 μM W146 s1PR1 antagonist blocked the effect of ASR396 on BK-mediated EC gap

formation, demonstrating ASR396 binding to S1PR1. (F) ASR396 and SEW2871 promoted S1PR1 internalization in HEK293A-S1P1-GFP cells, which was inhibited by S1PR1 antagonist W146. (G) The quantification of S1PR1 internalization following ASR396 and SEW2871 treatment of HEK293A-S1P1-GFP cells. Internalization was inhibited by S1PR1 antagonist W146. (H) Inflammatory mediators and ASR396 modulated phosphorylation of MLC. BK, VEGF and IL-8 increased the pMLC levels on western blots, while ASR396 reduced the VEGF- and IL-8-triggered MLC phosphorylation. (I, J, & K) Modulation of EC layer gap formation by nanoASR396. NanoASR396 inhibited (H) VEGF-, (I) BK- and (J) IL-8 induced gap formation.

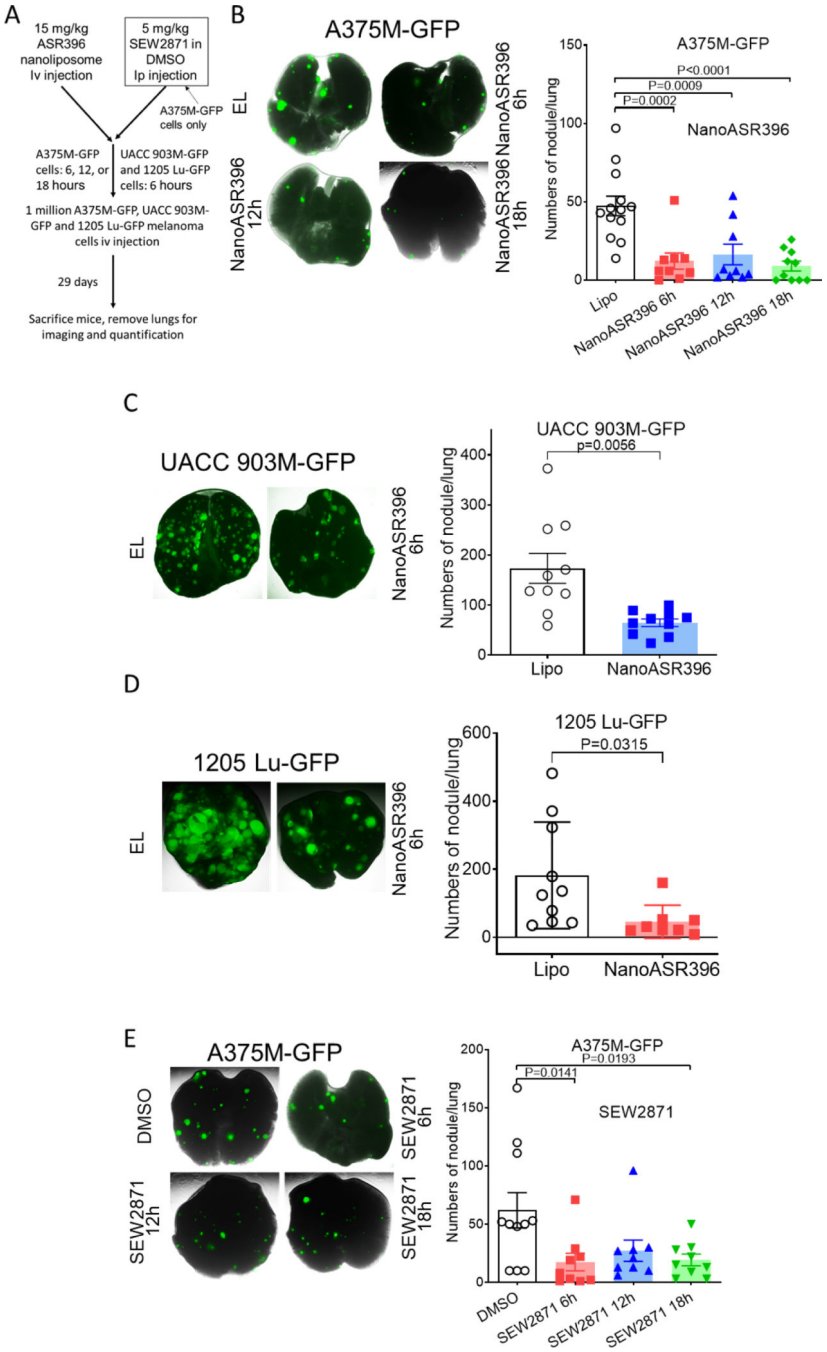

Figure 6. NanoASR396 inhibited melanoma lung metastasis.

(A) Overview of the treatments protocol to inhibit experimental melanoma cell metastasis. (B) 6, 12, or 18 hours prior to A375M-GFP melanoma cell injection, animals were treated with 15 mg/kg nanoASR396 and 29 days later GFP-tagged metastatic lung nodules quantified. Left: representative images of lungs under each treatment. Right: metastatic nodule quantification. (C) (D) 6 hours prior to UACC 903M-GFP and 1205 Lu-GFP melanoma cell injections, animals were treated with 15 mg/kg nanoASR396 and 29 days later GFP-tagged metastatic lung nodules quantified. Left: representative images of lungs

under each treatment. Right: metastatic nodule quantification. (E) 6, 12, or 18 hours prior to A375M-GFP melanoma cell injection, animals were treated with control intraperitoneally administered 5 mg/kg SEW2871 and 29 days later GFP-tagged metastatic lung nodules quantified. Left: representative images of lungs under each treatment. Right: metastatic nodule quantification.